Comparative analysis of quantum cascade laser modeling based on density matrices and non-equilibrium Green's functions

Franckie, Martin; Wolf, J. M.; Trinite, V.; Liverini, V.; Faist, J.; Maisons, G.; Carras, M.; Aidam, R.; Ostendorf, R.; Wacker, Andreas

Published in:
Applied Physics Letters

DOI:
10.1063/1.4895123

2014

Document Version:
Publisher's PDF, also known as Version of record

AIP | Applied Physics Letters

Comparative analysis of quantum cascade laser modeling based on density matrices and non-equilibrium Green's functions

M. Lindskog, J. M. Wolf, V. Trinite, V. Liverini, J. Faist, G. Maisons, M. Carras, R. Aidam, R. Ostendorf, and A. Wacker

Citation: Applied Physics Letters **105**, 103106 (2014); doi: 10.1063/1.4895123
View online: http://dx.doi.org/10.1063/1.4895123
View Table of Contents: http://scitation.aip.org/content/aip/journal/apl/105/10?ver=pdfcov
Published by the AIP Publishing

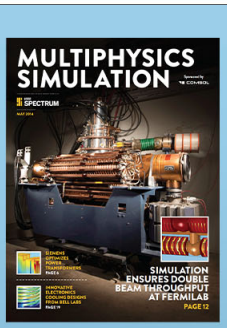

Comparative analysis of quantum cascade laser modeling based on density matrices and non-equilibrium Green's functions

M. Lindskog,[1,a)] J. M. Wolf,[2] V. Trinite,[3] V. Liverini,[2] J. Faist,[2] G. Maisons,[3] M. Carras,[3] R. Aidam,[4] R. Ostendorf,[4] and A. Wacker[1]
[1]*Mathematical Physics, Lund University, Box 118, 22100 Lund, Sweden*
[2]*ETH Institute for Quantum Electronics, ETH-Zürich, 8093 Zürich, Switzerland*
[3]*III-V Lab, 1 Avenue Augustin Fresnel, 91767 Palaiseau, France*
[4]*Fraunhofer-Institut für Angewandte Festkörperphysik, Tullastrasse 72, 79108 Freiburg, Germany*

(Received 18 July 2014; accepted 28 August 2014; published online 11 September 2014)

We study the operation of an 8.5 μm quantum cascade laser based on GaInAs/AlInAs lattice matched to InP using three different simulation models based on density matrix (DM) and non-equilibrium Green's function (NEGF) formulations. The latter advanced scheme serves as a validation for the simpler DM schemes and, at the same time, provides additional insight, such as the temperatures of the sub-band carrier distributions. We find that for the particular quantum cascade laser studied here, the behavior is well described by simple quantum mechanical estimates based on Fermi's golden rule. As a consequence, the DM model, which includes second order currents, agrees well with the NEGF results. Both these simulations are in accordance with previously reported data and a second regrown device. © *2014 AIP Publishing LLC*.
[http://dx.doi.org/10.1063/1.4895123]

Quantum cascade lasers[1] (QCLs) have become an important source of infra-red radiation for spectroscopy applications,[2] and different modeling techniques of varying level of detail have been used to simulate the performance of such structures.[3] The density matrix (DM) scheme,[4–6] where the transport is governed by scattering transitions and selected tunneling rates calculated from the off-diagonal elements of the density matrix, provides fast calculations in good agreement with experimental data.[7] This makes the DM model suitable for predicting the behavior of well-known QCL types, and allows for layer sequence optimization.[8] However, such models rely on a number of approximations, such as scattering mechanisms based on Fermi's golden rule and thermalized subbands, in order to form a consistent and efficient model.

In contrast to the DM scheme, the method of non-equilibrium Green's functions[9–12] (NEGF) takes into account the full coherences between the off diagonal elements of the density matrix, as well as scattering between states of different in-plane momentum k. Scattering effects are treated by matrices of self-energies,[9] which provides a self-consistent solution with the coherences mentioned above. Furthermore, the energetic widths of the states are fully included. However, the calculations are very resource-demanding, and thus put limitations on the structure optimization that is possible with such an approach. Instead, it is well suited to model well-defined problems in deep detail, since information about carrier, current, and state densities resolved in energy and space can be extracted from the Green's functions. The NEGF approach can thus be used to validate simpler models, as well as structures that have been optimized using these.

In this letter, we present simulations of a QCL[7] based on a GaInAs/AlInAs heterostructure lattice matched to InP under operation. We consider two implementations of the DM model, where the first (DM simp.) uses the first order current only, while the second one (DM 2nd), described in Refs. 6 and 13, includes the second order current following Ref. 14. These are directly compared with the NEGF model described in Ref. 15. The results are compared with experimental data from Ref. 7 and a regrowth reported here. Going beyond Ref. 16, where a similar comparison was done for another sample, we present simulations under lasing conditions as well.

The models used differ essentially with respect to the main concepts applied. For the DM models, the quantum electronic states are calculated for each period separately. The scattering transition rates between the states within the period are calculated by Fermi's golden rule. In addition, the tunneling rates between pairs of states of different periods are derived from a density matrix model. In contrast, the NEGF model uses a basis of Wannier functions, and treats all states on equal footing based on the microscopic Hamiltonian. The DM models have the areal electron densities of the specific levels and the coherences between them as principal variables. In order to evaluate the total transition rates, they assume a simple Fermi-Dirac distribution function with the same temperature for all sub-bands which is provided as an input. The full distribution with respect to k is resolved within the NEGF model, which is determined self-consistently, where the lattice temperature determines the occupation of the phonon modes. The only approximation is the use of momentum-independent effective scattering matrix elements, which highly simplifies the numerical scheme.[15] In the DM models, the optical transitions in the laser field are calculated via Fermi's golden rule where the energy-conserving delta-function is replaced by a Lorentzian. DM simp. uses an empirical broadening of 20 meV for the gain and the tunneling rates as an input to the program, whereas DM 2nd evaluates them with the Ando

[a)]Electronic mail: martin.lindskog@teorfys.lu.se

model.[13,17] In the NEGF model, gain is calculated from the dynamical conductance, and calculations in a strong ac field follow the procedure outlined in Ref. 18.

We consider scattering from interface roughness, longitudinal optical phonons, alloy disorder, acoustic phonons approximated by a single frequency (not used in DM 2nd), and ionized dopants (not used in DM simp.). Nonparabolicity in the band structure is treated via an effective two-band or three-band (for DM simp.) model.[19,20] All basic parameters, such as band gaps, effective masses and optical properties of the QCL materials, are the same in all models. For instance, all models use the same Gaussian interface roughness correlation length of 9 nm and height of 0.1 nm and a lattice temperature of 300 K. Additionally, in the DM models, the electron temperature was fixed to 430 K in contrast to the self-consistent calculation reported in Ref. 6. Inter-carrier Coulomb interaction is treated on a mean-field level.

We have simulated the structure described in Ref. 7 using the three models described above. The structure with the Wannier-Stark states is shown in Fig. 1, together with the carrier densities, which have a shift with respect to the Wannier-Stark states caused by impurity scattering.[21] These shifts mainly result from the real parts of the self-energies, which are of the order of 14 meV. They are similar for all states, so that they hardly affect the tunneling resonances.

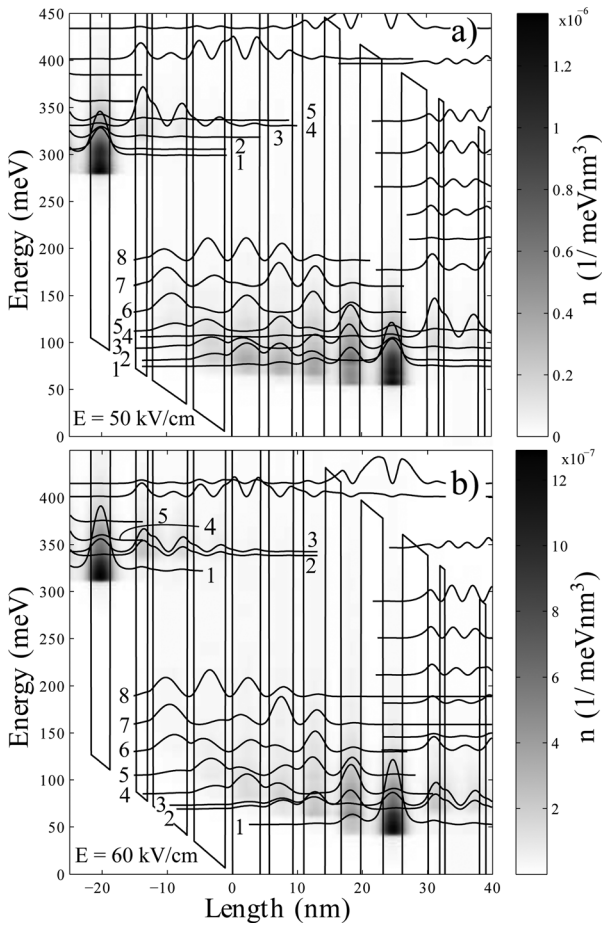

FIG. 1. Carrier densities and the square of the wave functions, calculated in the NEGF model, for different electric fields near threshold (a) and far above threshold (b). The numbers label the injection level (1), the upper laser levels (4 in (a), 2 and 3 in (b)), and the lower laser level (8).

Fig. 2 shows the current densities vs. applied electric field. The dashed lines show the experimental data for the original device and our regrowth, which agree until threshold ($J_{th} = 1.5$ kA/cm^2 and 2 kA/cm^2 of the original and regrown device, respectively). This reflects the reproducible growth quality as verified by X-ray measurements determining the actual period of 44.6 nm for the original and 44.7 nm for the regrown device (nominal 44.9 nm). In addition, the peak currents are comparable. The full lines give the simulation results of the different models without lasing. We see a good agreement between the NEGF model and the DM 2nd model for fields below ≈52 kV/cm, which both reproduce the experimental data below threshold. In contrast, as expected,[6] the DM simp. model provides a much larger current density, which shows the importance of including the second order current in the calculations.

The simulated gain spectra, taken in the limit of a vanishing lasing field, are shown in Fig. 3, near threshold (a) and far above threshold (b). The results of the DM 2nd and NEGF models agree near threshold while the DM simp. model shows a slightly larger gain with a blue-shift, coming from the approximation of constant effective mass in the gain calculation within this model. This trend is also seen in Fig. 3(c) for a wide range of electric fields, where the peak positions for both the NEGF and DM 2nd models agree qualitatively with the measurements. As the electric field increases, the gain evaluated by the two DM models increases strongly, while the NEGF model provides a significantly lower gain. This discrepancy most likely comes from the approximation of constant sub-band temperatures used in the DM models, while increasing electron temperatures provide detrimental occupation of higher levels at larger fields in the NEGF simulations. Another contributing factor is the restriction of the basis states to one period, which explains that the 1→8 side peak in Fig. 3(b) is not visible in the DM models. As can be seen in Fig. 1(a), the relevant upper laser level at threshold is level 4. At the higher field, however, the levels responsible for lasing are the two resonant levels

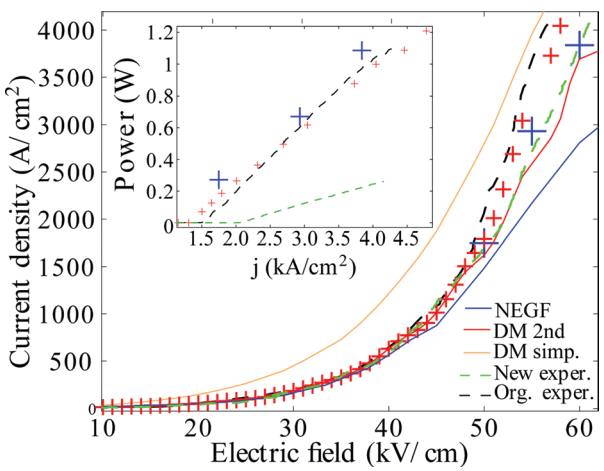

FIG. 2. Current-field characteristics for the different simulation models and experimental measurements. The field of the experimental data is obtained from the bias divided by the nominal length. Simulations under lasing conditions are given by large blue crosses for the NEGF and small red crosses for the DM 2nd model. The inset shows the measured and calculated output power as a function of the current density.

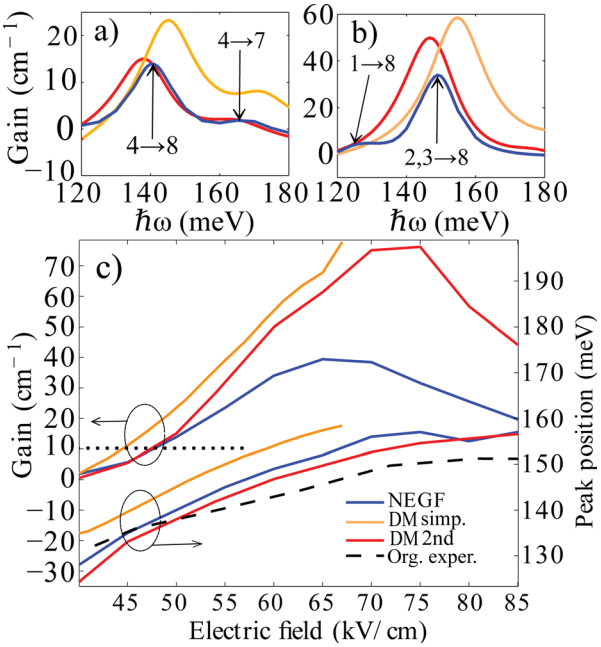

FIG. 3. Simulated spectral gain at electric fields of (a) 50 kV/cm and (b) 60 kV/cm. The gain is calculated in the off-state of the laser. In (a) and (b), the transitions of the respective gain peaks in the NEGF simulations are indicated. (c) Peak values and positions vs. electric field. The horizontal dotted line shows the computed threshold gain G_{th} for the original experiment. The experimental peak position (black dashes) is taken from the electroluminescence spectrum of Ref. 7.

2 and 3, whose coherence is only fully taken into account in the NEGF model.

The waveguide losses α_w for the device in Ref. 7 are reported to be 2.8 cm^{-1}. With a mirror loss of $\alpha_m = 3.3$ cm^{-1} and a mode confinement factor of $\Gamma_{\text{conf.}} = 0.63$, a gain $G_{\text{th}} \approx 10$ cm^{-1} is required in the QCL active region for achieving lasing. From Fig. 3(c), it is seen that in the DM 2nd and NEGF models, G_{th} is reached at $E_{\text{th}} = 47.3$ kV/cm and $E_{\text{th}} = 47.6$ kV/cm, respectively. This is in very good agreement with the experimental value of 48 kV/cm. For this field, the NEGF model provides a threshold current density of 1.2 kA/cm^2, and the DM 2nd model gives 1.3 kA/cm^2 (Exp. 1.5 kA/cm^2). Again, the DM simp. model differs, giving a threshold field of 44 kV/cm with the corresponding current density of 1.7 kA/cm. As the new device was processed using a double trench waveguide instead of the buried heterostructure technique used in the original device, the losses for this sample are higher. The observed threshold field of 52 kV/cm and threshold current of ≈2 kA/cm^2 reflect the trend for the gain simulations.

Under laser operation, an output power of $P = 0.5 - 1$ W was reported in Ref. 7. Using the relation for a traveling wave[18]

$$P = (F_{\text{ac}})^2 \frac{n_r c \varepsilon_0 A (1-R)}{2\Gamma_{\text{conf.}}}, \qquad (1)$$

where n_r is the refractive index of the gain medium, A is the facet area, and R is the reflectivity, we obtain an ac field inside the active region of strength $F_{\text{ac}}d \approx 100 - 130$ mV, where d is the period length. This is a significant amount compared with the dc field under operation $F_{\text{dc}}d \sim 250$ mV. This ac field is affecting the transport by increasing the current density above threshold, as expected in the case of photon-driven transport.[22] The simulated transport under an applied ac field is shown in Fig. 4, where an increasing $F_{\text{ac}}d$ results in an increased current density and a decreasing gain. For $F_{\text{dc}} = 50$ kV/cm, the NEGF results agree well with the DM 2nd model. Again, for $F_{\text{dc}} = 60$ kV/cm, the gain is higher for the DM model. The dotted line in Fig. 4 indicates G_{th} for the original device. Its intersection with the gain determines the ac field where gain and losses compensate. For these ac fields, Fig. 2 shows with crosses the NEGF and DM 2nd current densities under operation. This is in much better agreement with the experimental current density as compared to the simulations without a laser field. The corresponding power output (inset of Fig. 2) calculated from Eq. (1) for the NEGF model also agrees well with this experimental data as well as the DM 2nd model.

Now, we show that the gain in the NEGF model follows simple estimates, which demonstrates that the behavior can be understood in conventional terms. A simple calculation using Fermi's golden rule provides (see, e.g., Refs. 13 and 23)

$$G(\omega) = \frac{e^2 \Delta n_{fi} \Delta E_{fi}^2 z_{fi}^2}{2\hbar^2 \omega n_r c \epsilon_0 d} \frac{\Gamma_{\text{w}}}{\left(\Delta E_{fi} - \hbar\omega\right)^2 + \Gamma_{\text{w}}^2/4}, \qquad (2)$$

where Δn_{fi} is the inversion, $z_{fi} = 2.2$ the dipole matrix element, and ΔE_{fi} the energy difference for the final (f) and initial (i) states for the main gain transition. $\Gamma_{\text{w}} = 14$ meV is the FWHM of the gain spectrum from Fig. 3(a). Extracting the values Δn_{fi}, ΔE_{fi}, and z_{fi} from the NEGF simulations, we calculate for electric fields of 50 and 60 kV/cm a peak gain of 16 and 43 cm^{-1}, respectively, agreeing reasonably well with Figs. 3(a) and 3(b). Thus, the gain can be solely explained by the relationship (2), where Δn_{fi} accounts for the largest fraction of the variation in gain. This, together with the fact that the frequency of peak gain agrees with the energy difference between the peaks in the spectral function, shows that in this particular case, complex effects such as dispersive gain[24,25] and depolarization shifts[26,27] are not of

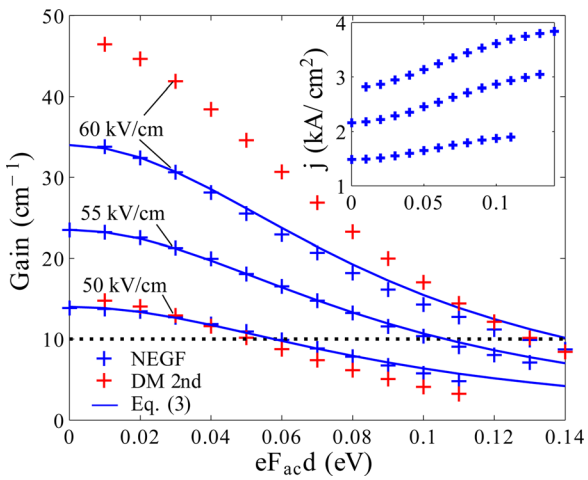

FIG. 4. Gain vs. applied ac field strength for different dc fields, simulated in the NEGF and DM 2nd models, compared to the relationship (3). The inset shows the current density in the NEGF model. The horizontal dotted line shows the threshold gain G_{th} of the original sample.

relevance. The differences in gain between the NEGF and the DM models for high dc fields can be attributed to the differences in Δn_{fi} addressed above.

Regarding the F_{ac} dependence in Fig. 4, it is reasonable to assume that the inversion drops proportionally to the product of gain times lasing intensity. Thus, we expect $G(F_{ac}) = G_0 - bG(F_{ac}) \times (F_{ac}d)^2$, where G_0 is the gain at zero field. The parameter b can be evaluated using Eq. (2) and standard kinetics, providing

$$G(F_{ac}) = \frac{G_0}{1 + b(F_{ac}d)^2} \quad \text{with} \quad b = \frac{\tau e^2 z_{fi}^2}{\hbar \Gamma_w d^2}. \tag{3}$$

We obtain $b = 120\,\mathrm{V}^{-2}$ for $z_{fi} = 2.2\,\mathrm{nm}$ and $\tau = 0.47$ ps (approximately the lifetime of the upper laser state). Fig. 4 shows that Eq. (3) reproduces the full NEGF calculations.

From the NEGF modeling results, the carrier densities for each level α and in-plane momentum k can be extracted. Fitting to a Fermi distribution function, the subband temperatures T_α can be extracted. With $E = 55\,\mathrm{kV/cm}$ without a lasing field, the upper laser state temperature $T_{ULS} = 398$ K is close to the electron temperature of 430 K used in the DM simulations, while the lower laser state temperature $T_{LLS} = 345$ K is significantly lower. When the laser field is turned on, with $F_{ac}d = 110$ mV, $T_{ULS} = 512$ K is now larger, while $T_{LLS} = 411$ K is close to the DM temperature instead.

In conclusion, we have presented simulations of a QCL both with and without a laser field, based on DM and NEGF models, and compared these results to experimental data from two separate growths. The transport and gain characteristics are well explained by simple relations, and thus, the DM 2nd model reproduces the experimental data as well as the NEGF model. However, the NEGF model predicts significantly lower gain and current for large dc fields close to the current density peak. We also find that the DM simp. model overestimates the current density in the devices, confirming the importance of taking the second order current into account. Finally, electron temperatures similar to those assumed in the DM models have been calculated using the NEGF model.

The research leading to these results has received funding from the European Union Seventh Framework Programme (FP7/2007-2013) under Grant Agreement No. 317884, the collaborative Integrated Project MIRIFISENS.

[1]J. Faist, F. Capasso, D. L. Sivco, C. Sirtori, A. L. Hutchinson, and A. Y. Cho, Science **264**, 553 (1994).
[2]R. F. Curl, F. Capasso, C. Gmachl, A. A. Kosterev, B. McManus, R. Lewicki, M. Pusharsky, G. Wysocki, and F. K. Tittel, Chem. Phys. Lett. **487**, 1 (2010).
[3]C. Jirauchek and T. Kubis, Appl. Phys. Rev. **1**, 011307 (2014).
[4]S. Kumar and Q. Hu, Phys. Rev. B **80**, 245316 (2009).
[5]E. Dupont, S. Fathololoumi, and H. C. Liu, Phys. Rev. B **81**, 205311 (2010).
[6]R. Terazzi and J. Faist, New J. Phys. **12**, 033045 (2010).
[7]A. Bismuto, R. Terazzi, M. Beck, and J. Faist, Appl. Phys. Lett. **96**, 141105 (2010).
[8]A. Bismuto, R. Terazzi, B. Hinkov, M. Beck, and J. Faist, Appl. Phys. Lett. **101**, 021103 (2012).
[9]S.-C. Lee, F. Banit, M. Woerner, and A. Wacker, Phys. Rev. B **73**, 245320 (2006).
[10]T. Schmielau and M. Pereira, Appl. Phys. Lett. **95**, 231111 (2009).
[11]T. Kubis, C. Yeh, P. Vogl, A. Benz, G. Fasching, and C. Deutsch, Phys. Rev. B **79**, 195323 (2009).
[12]G. Haldaś, A. Kolek, and I. Tralle, IEEE J. Quantum Electron. **47**, 878 (2011).
[13]R. Terazzi, *Transport in Quantum Cascade Lasers*, Ph.D. thesis, ETH Zürich, 2011.
[14]R. Terazzi, T. Gresch, A. Wittmann, and J. Faist, Phys. Rev. B **78**, 155328 (2008).
[15]A. Wacker, M. Lindskog, and D. Winge, IEEE J. Sel. Top. Quantum Electron. **19**, 1200611 (2013).
[16]P. Friedli, H. Sigg, A. Wittmann, R. Terazzi, M. Beck, A. Kolek, and J. Faist, Appl. Phys. Lett. **102**, 012112 (2013).
[17]T. Ando, J. Phys. Soc. Jpn. **54**, 2671 (1985).
[18]D. O. Winge, M. Lindskog, and A. Wacker, Opt. Express **22**, 18389 (2014).
[19]C. Sirtori, F. Capasso, J. Faist, and S. Scandolo, Phys. Rev. B **50**, 8663 (1994).
[20]M. Lindskog, D. O. Winge, and A. Wacker, Proc. SPIE **8846**, 884603 (2013).
[21]C. Ndebeka-Bandou, A. Wacker, F. Carosella, R. Ferreira, and G. Bastard, Appl. Phys. Express **6**, 094101 (2013).
[22]H. Choi, L. Diehl, Z.-K. Wu, M. Giovannini, J. Faist, F. Capasso, and T. B. Norris, Phys. Rev. Lett. **100**, 167401 (2008).
[23]J. Faist, *Quantum Cascade Lasers* (Oxford University Press, Oxford, 2013).
[24]R. Terazzi, T. Gresch, M. Giovannini, N. Hoyler, N. Sekine, and J. Faist, Nat. Phys. **3**, 329 (2007).
[25]D. G. Revin, M. R. Soulby, J. W. Cockburn, Q. Yang, C. Manz, and J. Wagner, Appl. Phys. Lett. **92**, 081110 (2008).
[26]P. Hyldgaard and J. W. Wilkins, Phys. Rev. B **53**, 6889 (1996).
[27]M. F. Pereira, Jr., S.-C. Lee, and A. Wacker, Phys. Rev. B **69**, 205310 (2004).